Photomechanical Energy Transfer to Photopassive Polymers through Hydrogen and Halogen Bonds

Jaana Vapaavuori,*[,†] Ismo T. S. Heikkinen,[†,‡] Valentina Dichiarante,[§] Giuseppe Resnati,[§] Pierangelo Metrangolo,[§] Ribal Georges Sabat,[∥] C. Geraldine Bazuin,[†] Arri Priimagi,*[,⊥] and Christian Pellerin*[,†]

[†]Département de chimie, Centre de Recherche sur les Matériaux Auto-assemblés (CRMAA/CSACS), Université de Montréal, C.P. 6128, Succ. Centre-Ville, Montréal, QC, Canada H3C 3J7

[‡]Department of Applied Physics, Aalto University, P.O. BOX 13500, FI-00076 Aalto, Finland

[§]NFMLab-DCMIC "Giulio Natta", Politecnico di Milano, Via L. Mancinelli 7, IT-20131 Milano, Italy

[∥]Department of Physics, Royal Military College of Canada, Kingston, ON, Canada K7K 7B4

[⊥]Department of Chemistry and Bioengineering, Tampere University of Technology, P.O. Box 541, FI-33101 Tampere, Finland

Received: August 16, 2015
Revised: September 25, 2015
Published: October 5, 2015

INTRODUCTION

Azobenzene molecules can translate the energy of light directly into motion in a well-controlled manner through the *trans*−*cis* photoisomerization reaction.[1−3] Photoisomerization can further be used to control the motion of passive nonabsorbing molecules, such as liquid crystals and polymers, which is of fundamental interest not only for new light-energy conversion systems but also for molecular-level engineering of material properties. Azobenzenes can power movements at three different length scales: at the molecular, domain, and macroscopic levels.[3] As an illustrative molecular-level example of manipulating passive molecules, the photoisomerization of the azobenzene can twist a supramolecularly attached guest molecule located between imidazole-based photoresponsive tweezers.[4] At the domain level, azobenzene photoswitching has been successfully employed to provoke the isothermal phase transition of various liquid crystalline phases into an isotropic phase[5,6] and to photocontrol the orientation of macrophase-separated domains in liquid-crystalline block copolymers.[7,8] On the macroscopic scale, the mass transport upon illumination by inhomogeneous light patterns to generate surface relief gratings (SRG)[9,10] and the macroscopic bending of free-standing films of cross-linked liquid-crystalline polymers and elastomers can be achieved in the solid state for azo-containing materials.[11,12]

Arguably, the easiest way to couple azobenzenes to photopassive polymers is through spontaneous formation of supramolecular bonds between complementary molecular moieties. Such noncovalent bonds can kinetically "trap" the azobenzene molecules, thus preventing or slowing their relatively strong tendency to crystallize, which is detrimental to the optical properties.[13] The literature abounds with examples of different supramolecular synthons forming ionic,[14−19] hydrogen,[20−24] and halogen[25−27] bonds to construct a variety of photoresponsive materials. However, a comprehensive fundamental understanding of the nature and impact of the bonding type and strength in controlling the motion of

passive polymer hosts has not yet been established. It is of special interest to investigate the stability of these supramolecular bonds under repetitive *trans*−*cis*−*trans* isomerization cycles.

Analogously to hydrogen bonding, halogen bonding is the interaction between the positive outer region of an electrophilic halogen atom and a nucleophile.[28] A particular feature of both halogen and hydrogen bonding is that they form dynamic equilibrium structures, allowing precise tuning of the relative amounts of passive and active units in the materials. These supramolecular bonds are also advantageous for their simple sample preparation and for their relatively low sensitivity to humidity as compared to ionic bonding. Furthermore, in contrast to covalent bonds, they enable dynamic bond formation and breaking, which may be advantageous in terms of photomechanical performance[29] and for applications in which transparency is needed, since the active units can be detached by selective solvation after they have completed their function.[30]

Although they share many common features, halogen bonding differs from hydrogen bonding in a few important ways.[30] Most importantly, the positive electrostatic potential of a halogen-bond donor (X) is typically centered along the extension of the R−X bond, thus preserving the linearity of the whole supramolecular complex (when both starting molecules are linear). In contrast, the bond angle for hydrogen bonding of medium or weak strength is typically less than 180°.[31,32] Recently, it has been demonstrated that halogen-bonded polymer−azobenzene complexes surpass their hydrogen-bonded counterparts in the efficiency of photoinduced SRG formation, suggesting that the directionality difference between these two bonding types plays an important role in determining the photomechanical behavior of these materials.[26]

The most common method to study the photo-orientation of azo-containing materials upon illumination with linearly polarized light is to measure their birefringence or dichroism at UV−visible wavelengths. However, a more informative method for following photoinduced motions, especially when passive molecules are involved, is infrared (IR) spectroscopy because it allows independent tracking of different molecular groups.[3,33] Pézolet and co-workers have shown that polarization modulation infrared linear dichroism (PM-IRLD) can measure photoinduced orientation with higher accuracy and with significantly enhanced time resolution as compared to that with conventional IRLD.[34,35] This technique was applied to show, for instance, that in random copolymers containing azobenzene and nonphotoactive side chains the passive side chains can orient alongside the azobenzenes due to dipole−dipole interactions.[36] Liang and co-workers later developed an improved implementation of PM-IRLD, using identical instrumentation, called polarization modulation IR structural absorbance spectroscopy (PM-IRSAS).[37] This technique enables the two individual polarized spectra to be measured simultaneously, in addition to their dichroic difference, and therefore provides the time-resolved structural absorption spectra. As a consequence, PM-IRSAS preserves the time resolution and sensitivity of PM-IRLD but extends its capabilities by providing additional structural information on intermolecular interactions, conformation, crystallinity, and so forth. Although different intramolecular chromophore−chromophore interactions have been studied by IR in covalent side-chain polymers, to the best of our knowledge, it has not yet been applied to supramolecular systems, in which dynamic intermolecular interactions play a key role in the formation, stability, and performance.

In this article, we employ PM-IRSAS to establish a correlation between the movements of the azobenzenes at the molecular level and the macroscopic phenomenon of SRG photopatterning in halogen- and hydrogen-bonded supramolecular materials. We show that there is a threshold, both in the concentration of photoactive azobenzenes and in the strength of the supramolecular interaction, that must be surpassed to induce the orientation of a photopassive polymer. For sufficiently strong interactions, the dynamic equilibrium of formation and dissociation of supramolecular bonds is only slightly shifted toward bond breaking by the vigorous switching between *trans* and *cis* states, and the supramolecular bonds can thus be regarded as photostable enough to transmit the orientation of the azobenzene to the polymer. In the halogen-bonded complex, both the azobenzene moiety and the polymer orient better than in the corresponding hydrogen-bonded complex, which can be linked to its better SRG formation capability. In addition, it was found that the halogen-bonded molecule does not affect the polymer mobility when it is incorporated into the polymer matrix, resulting in a glass transition temperature that is significantly higher than that for the analogous hydrogen-bonded complex.

EXPERIMENTAL SECTION

Azobenzenes **1** and **3** were synthesized following the procedure described previously.[25] Azobenzenes **2** and **4** were purchased from Tokyo Chemical Industries, poly(4-vinylpyridine) (P4VP with M_n = 3200 g/mol) was purchased from Polymer Source, and they were used as received. Samples for IR and SRG measurements were prepared from 2 wt % azobenzene solutions and a 15 wt % P4VP solution in tetrahydrofuran, whereas samples for the UV−visible measurements were made using 1 wt % azobenzene and 10 wt % P4VP solutions. The stock solutions were mixed to have complexation degrees of 0.10 and 0.25 (azo/VP molar ratios). This resulted in approximately 6 wt % complex solutions for IR samples and 2 wt % solutions for UV−visible samples. Thin film samples were spin-coated at a speed of 1000 rpm for 60 s on KBr substrates for IR and on conventional microscope slides for SRG and UV−visible studies.

UV−visible spectra were recorded with an Ocean Optics USB2000+ spectrophotometer and a DH-mini light source, and a linearly polarized 488 nm diode laser (JDSU FCD488-020) was used to induce photoisomerization in the sample. A Bruker Optics Vertex 70 Fourier transform IR spectrometer was used to measure static transmission spectra and dynamic PM-IRSAS spectra at a 4 cm^{-1} resolution. In the PM-IRSAS setup (represented in Scheme S1 of the Supporting Information), the IR beam is led to the sample at normal incidence through a linear polarizer and a photoelastic modulator (PEM-90, type II/ZS50, Hinds Instruments), which changes the polarization of the IR beam from parallel to perpendicular with respect to the pump laser polarization at 100 kHz. The signal was recorded with a liquid nitrogen-cooled photovoltaic mercury−cadmium−telluride (MCT) detector (Kolmar Technologies). A lock-in amplifier (Stanford Research Systems SR830) with a 30 μs time constant and electronic filters (Frequency Devices 90TP/90IPB) were used to isolate the experimental signals.[37] The PM-IRSAS setup was combined with the 488 nm laser used in the UV−visible experiments to induce photo-orientation. The diameter of the vertically polarized laser beam was expanded to ∼7 mm (Thorlabs BE10M-A) to overfill the IR probe beam (∼1 mm) and was incident on the sample at an angle of 20°. A 160 mW/cm^2 LED source (Prizmatix FC5-LED) operating at 450 nm was used for studying the photostability of the films under nonpolarized light.

To write the SRGs, a Lloyd's mirror interferometer, the mirror making an angle of 14° with respect to the laser beam, was used to produce the interference pattern with an Ar^+ laser source operating at

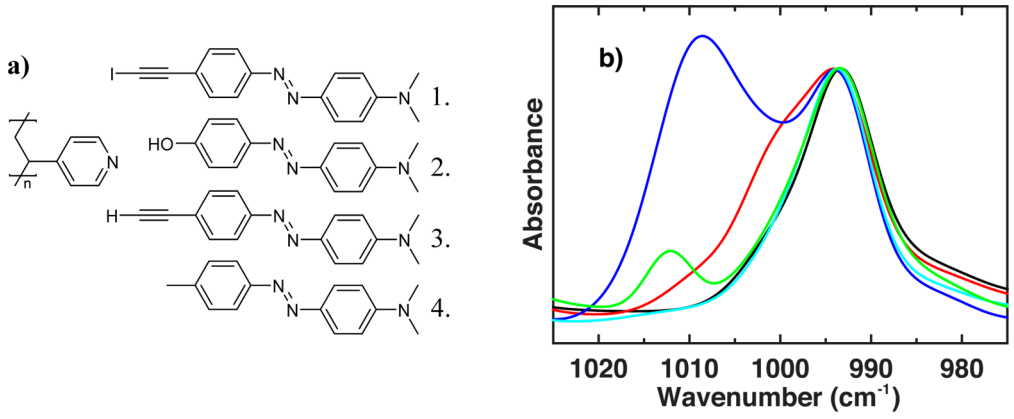

Figure 1. (a) Molecular structures of the complexes studied. (b) IR spectra of the pyridine stretching vibration in pure spin-coated P4VP (black), $\mathbf{p}(\mathbf{1})_{0.25}$ (red), $\mathbf{p}(\mathbf{2})_{0.25}$ (blue), $\mathbf{p}(\mathbf{3})_{0.25}$ (cyan), and $\mathbf{p}(\mathbf{4})_{0.25}$ (green).

488 nm at approximately 50 mW/cm^2 irradiance. The beam was made circularly polarized with the help of a quarter-wave plate. The first-order diffraction efficiency upon SRG formation was measured with a low-power HeNe laser (633 nm), which is not absorbed by the samples.

DFT calculation of the dipole moments were made on the Briarée supercomputer from Université de Montréal using the pbepbe functional with a 6-311++g(d,p) basis set.

RESULTS AND DISCUSSION

To bridge the gap in the understanding of photoinduced motions in halogen- and hydrogen-bonded azobenzene-containing systems and to address the general question of the stability of these relatively weak bonds under illumination, we studied *in situ* the photo-orientation and the interactions of the library of molecules presented in Figure 1a. Chromophore **1** is a halogen-bond donor, and chromophores **2** and **3** are hydrogen-bond donors to the pyridine group of the polymer used, poly(4-vinylpyridine) (P4VP, also referred to as **p**), whereas chromophore **4** serves as a nonbonding reference. The molar ratios of the azo molecules relative to the polymer repeat units in the complexes were either 0.25 or 0.10. DFT calculations[26] predict that the interaction strength of the extensively studied phenol−pyridine hydrogen bond between **2** and **p** (−10.05 kcal/mol) is twice the halogen-bonding interaction strength between **1** and **p** (−5.17 kcal/mol). The calculated interaction strength between the terminal hydrogen (vicinal to the triple bond) in **3** and the pyridine in **p** is weaker, at −3.53 kcal/mol,[26] since the hydrogen in **3** is not attached to a strongly electronegative atom. All of these P4VP−azobenzene complexes were shown to form SRGs when exposed to light interference patterns, in the efficiency order **1** > **2** > **3**, thus implying that the type of supramolecular interaction plays a key role in macroscopic manipulation of supramolecular poly-mers.[26]

The formation of supramolecular interactions between chromophores **1**−**4** and P4VP was first investigated by following the pyridine stretching vibration that is known to shift from 993 cm^{-1} for free pyridine to higher wavenumbers depending on the bonding strength.[38] As shown in Figure 1b, halogen bonding of pyridine with **1** shifts this band to approximately 1002 cm^{-1} (based on second-derivative anal-ysis), whereas hydrogen bonding with **2** results in a larger shift to 1009 cm^{-1} due to its greater interaction strength. The band associated with uncomplexed pyridine is evident in both spectra due to the relatively low azobenzene/polymer ratio used (0.25:1). Doping **p** with **3** or **4** results in a negligible pyridine band shift, less than 1 cm^{-1}. This was expected for $\mathbf{p}(\mathbf{4})_{0.25}$ because chromophore **4** does not bond specifically to pyridine.[It should be noted that the band at 1013 cm^{-1} observed for $\mathbf{p}(\mathbf{4})_{0.25}$ is also present in the spectrum of pure **4** and should not be interpreted as resulting from pyridine vibration shifting.] For $\mathbf{p}(\mathbf{3})_{0.25}$, the lack of significant shift suggests that if the supramolecular interaction takes place then it is not as strong as indicated by the calculations and/or that it is only partial. This can be rationalized by the fact that the calculations predicting the interaction strengths were done in vacuum and thus did not take into account competing interactions, such as $\pi-\pi$ stacking and dipole−dipole interactions, which are present in the solid state and may have interaction strengths of the same order of magnitude as that between **p** and **3**. It may be argued that shifts of the pyridine band could be caused by an increase in free volume due to plasticization by the chromophores that decreases the glass transition temperature (T_g) of the mixtures. This should have the same spectroscopic effect as heating the polymer; however, as shown in Figure S1, the 993 cm^{-1} pyridine band shifts toward lower wavenumbers upon heating and thus the observed shifts cannot be attributed to a plasticization effect. In summary, chromophores **1** and **2**, having higher interaction strengths, create supramolecular complexes with P4VP efficiently, whereas **3** and **4** have weak or no specific interactions with P4VP.

UV−visible spectroscopy was employed (Figure 2) to determine if the chromophores, especially nonbonded **3** and **4**, are molecularly dispersed or aggregated in the polymer matrix. Figure 2 shows the normalized spectra of the studied

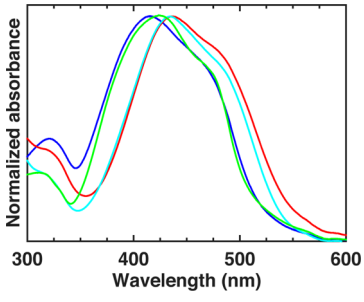

Figure 2. Normalized UV−visible absorption spectra of spin-coated films of $\mathbf{p}(\mathbf{1})_{0.25}$ (red), $\mathbf{p}(\mathbf{2})_{0.25}$ (blue), $\mathbf{p}(\mathbf{3})_{0.25}$ (cyan), and $\mathbf{p}(\mathbf{4})_{0.25}$ (green).

complexes in spin-coated thin films. No evidence of chromophore−chromophore aggregation is found for $\mathbf{p(1)}_{0.25}$, $\mathbf{p(2)}_{0.25}$, and $\mathbf{p(3)}_{0.25}$ because these thin films retain the same maximum wavelength for the main absorption as compared to that of the pure dyes in solution (Figure S2 shows an example for $\mathbf{p(3)}_{0.25}$ and pure **3** in $CHCl_3$). In addition, the thin films of these three complexes were clear and uniform, with spectra measured in different areas of the film being identical. In contrast, thin films of $\mathbf{p(4)}_{0.25}$ appeared cloudy, and the shape of the spectra depended on location, as demonstrated in Figure S3. Thus, it can be concluded that chromophores **1**−**3** are well-dispersed in the P4VP matrix at least up to a 0.25 molar ratio, preventing their crystallization, whereas chromophore **4** shows some molecular aggregation. The molecular dispersion of **3** in $\mathbf{p(3)}_{0.25}$, for which hydrogen bonding could not be observed by IR, is supported by the terminal alkyne C−H stretching band in the IR spectrum that shows no evidence of crystallization (see Figure S4).

From a photochemical point of view, the UV−visible spectra of $\mathbf{p(1)}_{0.25}$ and $\mathbf{p(3)}_{0.25}$ are red-shifted compared to those of $\mathbf{p(2)}_{0.25}$ and $\mathbf{p(4)}_{0.25}$ due to their longer conjugation length and higher electrostatic ground-state dipole moments (Table 1).

Table 1. Thermal, Electrical, and UV−Visible Spectral Characteristics of the Compounds Studied

compound	calculated dipole moment of the pure dye (D)	λ_{max} (nm)	A_{pss}/A_{init} [a]	T_g (°C)
$\mathbf{p(1)}_{0.25}$	6.37	436	0.73	88
$\mathbf{p(2)}_{0.25}$	4.13	415	0.93	67
$\mathbf{p(3)}_{0.25}$	6.31	434	0.73	50
$\mathbf{p(4)}_{0.25}$	3.45	419	0.77	62
p (3200 g/mol)				87

[a] A_{pss}/A_{init} is the ratio of absorbances at λ_{max} of the photostationary and initial states and is indicative of the minimum *cis* content in the photostationary state.

When irradiating thin films of the samples with 6 mW/cm^2 of linearly polarized 488 nm light, a decrease in the UV−visible absorption was observed. The extent of this drop in the absorbance of the *trans* isomer can be used to estimate the lower limit of *cis* content in the photostationary state, listed in Table 1. The photostationary *cis* content is only 7% for $\mathbf{p(2)}_{0.25}$, compared to 23−27% for the other compounds, which can be explained by the faster *cis* relaxation (shorter *cis* half-life) for chromophore **2** as compared to that of the other chromophores.[26] Although the absorption coefficients of the four compounds are somewhat different at 488 nm, illumination at that wavelength presumably excites the n−π^* transition of both *trans* and *cis* isomers for all of the chromophores studied, thus driving efficient *trans*−*cis*−*trans* cycling and furthermore rendering the materials comparable.

The addition of chromophores **1**−**4** in the P4VP matrix leads to surprisingly different thermal properties for the complexes (Table 1). The T_g of the pure (low molecular weight) P4VP used is 87 °C. Chromophores **1** and **3**, which have identical structures except for the terminal atom on the ethynyl group, give rise to the two extreme effects of not changing the T_g at all and of reducing it the most strongly (by more than 35 °C), respectively. Chromophores **2** and **4** have an intermediate effect, reducing the P4VP T_g by 20 and 25 °C, respectively. Such contrasting effects on the T_g can be related to differences in interaction type and strength, azobenzene molecular structure, and dispersion of the chromophores. The bulkiness of the iodine moiety in **1** compared to the terminal proton in **3**, combined with the strong and linear halogen bonding of **1** to pyridine compared to the weak binding of **3**, but where both are well-dispersed in the matrix, results in chromophore **1** introducing no additional mobility into the system, whereas chromophore **3** has a strong plasticizing effect. The somewhat lesser plasticizing effect of **2** compared to that of **4** can be related mainly to the good dispersion of **2** in the matrix due to its efficient H-bonding with P4VP. Chromophore **4** might, in fact, have had a stronger plasticizing effect if it were well-dispersed (perhaps even more than **3** considering the latter's rigid ethynyl moiety), but this is attenuated by its aggregation within the matrix, as indicated above. The greater plasticization by **2** compared to that by **1**, despite the greater interaction strength of **2** with P4VP, may be related to the nonlinear nature of the hydrogen-bonded supramolecular structures (in terms of azimuthal angle of the hydrogen bond) compared to the halogen-bonded ones, in addition to the greater mobility of the OH group (dihedral angle around the C−O bond) as compared to the rigid iodoethynyl motif.

The photo-orientation of the azobenzene and of P4VP in the different complexes under linearly polarized 488 nm light was studied selectively *in situ* by PM-IRSAS. An azobenzene band at 1137 cm^{-1} for **1**, 1148 cm^{-1} for **2**, 1138 cm^{-1} for **3**, and 1140 cm^{-1} for **4** and a P4VP band at 1220 cm^{-1} were selected as representative, relatively well-resolved bands for analysis. These bands are the result of complex ring deformation modes, but DFT calculations indicate that the transition dipole moment of the selected azobenzene bands points along the main axis of the dye, whereas that of the P4VP band is along the C1−N axis of the pyridine ring. To quantify the photo-orientation, the order parameter, T_2, was calculated as

$$T_2 = \frac{A_{\parallel} - A_{\perp}}{A_{\parallel} + 2A_{\perp}}$$

where $A_{\parallel}$ and $A_{\perp}$ are the absorbances parallel and perpendicular, respectively, to the polarization of the inscription beam.

Figure 3 plots the T_2 values for the azobenzene moiety in compounds $\mathbf{p(x)}_{0.25}$ as a function of time for 200 s after switching on the irradiation (at time 100 s) and then as a function of relaxation time for an additional 100 s. The kinetics of the photo-orientation process is similar for $\mathbf{p(1)}_{0.25}$, $\mathbf{p(2)}_{0.25}$, and $\mathbf{p(3)}_{0.25}$, where the azobenzenes are molecularly dispersed, with a very rapid initial increase in orientation in the first few

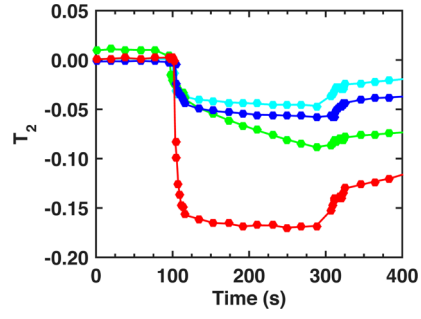

Figure 3. Time evolution of the photo-orientation (T_2) of the azobenzene moiety in $\mathbf{p(1)}_{0.25}$ (red), $\mathbf{p(2)}_{0.25}$ (blue), $\mathbf{p(3)}_{0.25}$ (cyan), and $\mathbf{p(4)}_{0.25}$ (green). Laser irradiation was switched on at 100 s and off at 300 s.

seconds followed by a much slower increase that tends toward saturation within 100 s of illumination. On the other hand, the T_2 value reached by the azobenzene in $\mathbf{p(1)}_{0.25}$ is much larger (in absolute terms) than that in $\mathbf{p(2)}_{0.25}$ and $\mathbf{p(3)}_{0.25}$ and follows the order of increasing T_g. A lower T_g implies shorter relaxation times for the polymer chains, leading to a competition between the photo-orientation and the counteracting orientation relaxation of the complexed or dispersed dyes. This is especially evident when comparing $\mathbf{p(1)}_{0.25}$ and $\mathbf{p(3)}_{0.25}$, whose T_g values differ strongly (Table 1) while their photochemistry, as given by their similar dipole moments, UV−visible absorption maxima, and *cis* concentration in the photostationary state, is essentially identical. As a first approximation, $\mathbf{p(1)}_{0.25}$ and $\mathbf{p(3)}_{0.25}$ can thus be regarded as containing the same dye at a different temperature relative to T_g, with $\mathbf{p(1)}_{0.25}$ having a T_g almost 40 °C higher than that of $\mathbf{p(3)}_{0.25}$. In addition, the saturation value of T_2 in halogen-bonded $\mathbf{p(1)}_{0.25}$ is approximately 3 times higher than the value for weakly interacting $\mathbf{p(3)}_{0.25}$, and the long-term stability of the orientation after turning off the illumination is 68% for $\mathbf{p(1)}_{0.25}$ and 41% for $\mathbf{p(3)}_{0.25}$ of the maximum T_2. Thus, a higher T_g appears to optimize both the level of saturated photoinduced anisotropy and its thermal stability. A similar beneficial effect of increasing T_g was observed previously when doping Disperse Red 1 in amorphous polymer matrices with different T_g values.[39] The results of Figure 3 support the rule of thumb that the anisotropic orientation of dyes is stable only when the operating temperature is more than 50 °C below the T_g, as established based on the study of poled polymer systems.[40]

The mechanism of photo-orientation is clearly different for $\mathbf{p(4)}_{0.25}$ compared to that of the other three complexes and is likely related to the molecular aggregation of **4** in P4VP. First, $\mathbf{p(4)}_{0.25}$ shows an initial orientation, as observed by the positive T_2 values before irradiation, that must have been induced by the spin-coating procedure, whereas the other three samples are initially isotropic. This initial orientation varies with location in the film, as did the UV−visible spectra of Figure S3, and can either lead to positive or negative initial T_2 values. The kinetics of photo-orientation of $\mathbf{p(4)}_{0.25}$ is also markedly different, showing no sign of saturation after 200 s of irradiation. It has been shown previously that the photo-orientation of azobenzene aggregates strongly depends on the irradiance used and that the achieved orientation is essentially stable,[41] as also observed in Figure 3 from the limited thermal relaxation of $\mathbf{p(4)}_{0.25}$. Although $\mathbf{p(4)}_{0.25}$ presents interesting photoactivity, controlling the formation and behavior of these aggregates reproducibly is more difficult than preparing molecularly dispersed samples, since the size of the aggregated molecular stacks depends strongly on the solvent evaporation rate and, thus, on the sample thickness and preparation conditions. In addition, the optical quality of the thin films is poor, since aggregates lead to light scattering and higher surface roughness. Such detrimental effects are more easily avoided when sufficiently strong halogen bonds or hydrogen bonds exist between the polymer and the dye.

Studying the orientation of the pyridine vibration at 1220 cm^{-1} reveals that a minimum interaction strength between the photoactive azobenzene and P4VP is required to convert light energy into polymer orientation. Indeed, polymer anisotropy was induced in $\mathbf{p(1)}_{0.25}$ and $\mathbf{p(2)}_{0.25}$, which have relatively strong supramolecular bonding, but not in $\mathbf{p(3)}_{0.25}$ and $\mathbf{p(4)}_{0.25}$, for which the supramolecular bonding is inexistent or very weak. In addition, the fact that **3** and **4** plasticize **p** more efficiently compared to **1** and **2**, as shown by the T_g values in Table 1 and discussed above, enhances the polymer relaxation process that would counteract any photo-orientation of the polymer chains. The significant orientation of the photopassive pyridine moiety induced by photo-orientation of the azobenzenes in $\mathbf{p(1)}_{0.25}$ and $\mathbf{p(2)}_{0.25}$ is shown by the saturated T_2 values reported in Table 2 for the azobenzene and pyridine groups. The negative T_2 values indicate that the C1−N axis of the pyridine side chain orients perpendicular to the laser polarization, as is expected considering the geometry of the supramolecular complexes. The orientation of the pyridine ring reached a plateau within 50 s of illumination and is more than twice as large for halogen-bonded $\mathbf{p(1)}_{0.25}$ compared to that for hydrogen-bonded $\mathbf{p(2)}_{0.25}$. This suggests a much more efficient energy transfer through the halogen bond in spite of its lower interaction strength. However, the comparison between these materials is complicated by the fact that the orientation of the driving azobenzene moiety is also much higher for **1** than for **2**. To take this factor into account, Table 2 also shows the percentage of pyridine orientation relative to the orientation of its driving azobenzene, from which it can be observed that the stronger interaction of the hydrogen bond in $\mathbf{p(2)}$ translates into a larger relative orientation of the polymer host. This relative pyridine orientation reflects the proportion of nominally bonded pyridines for $\mathbf{p(2)}_{0.25}$, whereas the orientation transfer is less efficient for $\mathbf{p(1)}_{0.25}$. However, it must be emphasized that the much higher orientation of **1** in $\mathbf{p(1)}_{0.25}$ makes this halogen-bonded dye more effective at driving the orientation of the photopassive polymer and, as will be shown below, at inscribing SRG patterns.

Table 2. Photo-Orientation (Saturated T_2 Values) of the Azobenzene and Pyridine Moieties in Halogen-Bonded p(1) and Hydrogen-Bonded p(2) Complexes

compound	T_2 (azobenzene)	T_2 (pyridine)	relative polymer orientation (%)
$\mathbf{p(1)}_{0.1}$	−0.26	−0.012	5
$\mathbf{p(1)}_{0.25}$	−0.17	−0.029	17
$\mathbf{p(2)}_{0.1}$	−0.08	−0.010	13
$\mathbf{p(2)}_{0.25}$	−0.05	−0.013	26

Table 2 also shows results for samples with a lower dye molar ratio, $\mathbf{p(1)}_{0.10}$ and $\mathbf{p(2)}_{0.10}$, which allow the minimum degree of doping necessary to orient pyridine groups and its impact on the orientation of both the azobenzene and polymer to be estimated. As expected, decreasing the degree of complexation decreases the orientation of the passive polymer chains. On the other hand, the lower dye content leads to a significant increase in azobenzene photo-orientation. This clearly shows that there is a trade-off between the achievable azobenzene and pyridine orientations.

Interestingly, for all of the complexes, no orientation was observed for the polymer backbone, as determined using the CH_2 stretching bands in the 2800−3000 cm^{-1} region (data not shown). This suggests that adapting the local conformation of the polymer side chains is energetically more favorable than reorienting a backbone segment to adjust to pyridine reorientation. This result is consistent with previous observations for polymers containing covalently bonded azobenzene side chains[42] and is not necessarily a consequence of the supramolecular nature of the complexes. It thus indicates that the picture in which the photo-orientation of the side-chain

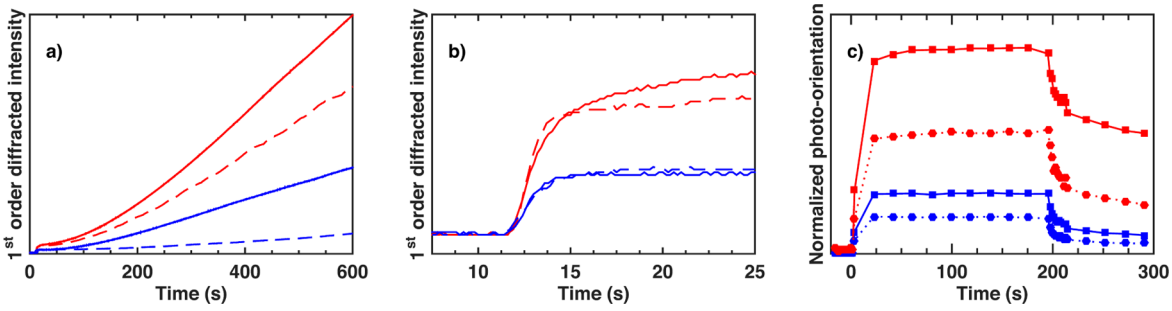

Figure 4. (a) Intensity of the first-order diffraction of a nonresonant 633 nm probe beam upon photopatterning spin-coated films of $\mathbf{p(1)}_{0.1}$ (dashed red), $\mathbf{p(1)}_{0.25}$ (plain red), $\mathbf{p(2)}_{0.1}$ (dashed blue), and $\mathbf{p(2)}_{0.25}$ (plain blue). (b) The early stage of panel (a). (c) Azobenzene photo-orientation normalized by the number of azobenzene molecules per polymer chain for $\mathbf{p(1)}_{0.1}$ (red circles), $\mathbf{p(1)}_{0.25}$ (red squares), $\mathbf{p(2)}_{0.1}$ (blue circles), and $\mathbf{p(2)}_{0.25}$ (blue squares).

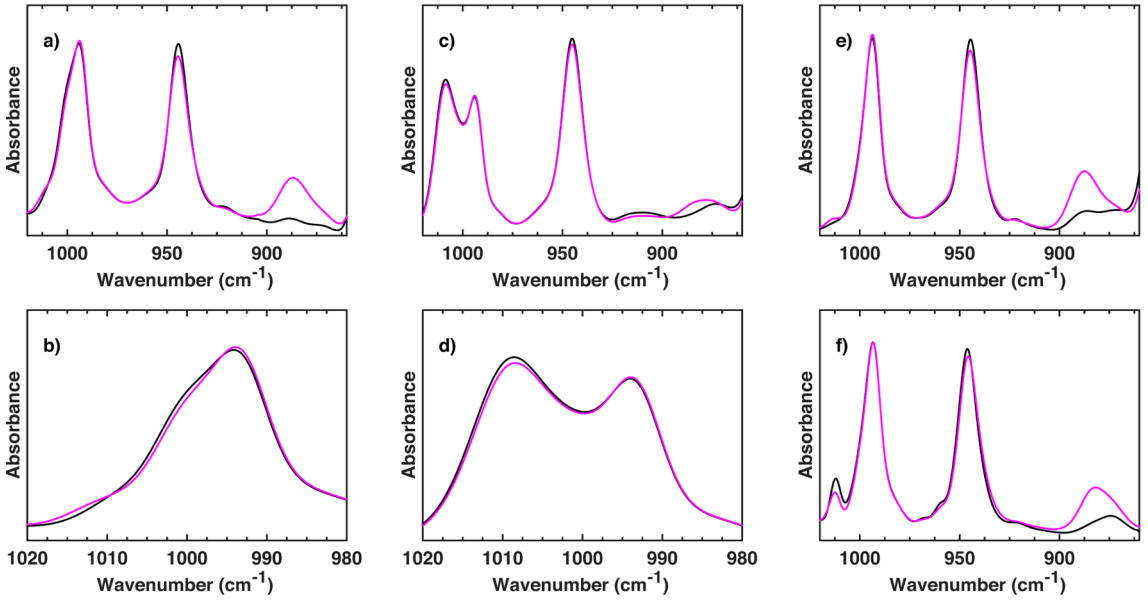

Figure 5. Static IR spectra recorded in the dark (black) and under (pink) illumination of 450 nm unpolarized light for (a, b) $\mathbf{p(1)}_{0.25}$, (c, d) $\mathbf{p(2)}_{0.25}$, (e) $\mathbf{p(3)}_{0.25}$, and (f) $\mathbf{p(4)}_{0.25}$.

azobenzene directly translates into rotation of the polymer backbone, often hypothesized in the literature,[43,44] is a simplification and suggests that a polymer with less rotational freedom than P4VP may be optimal for motion transfer. For instance, for a semicrystalline azopolymer in which the azo group is covalently bonded to the main chain without a spacer, an efficient translation of orientation from the side chains to the backbone resulted in impressive birefringence.[45]

It was previously shown that SRGs can be optically inscribed using $\mathbf{p(1)}_{0.10}$, $\mathbf{p(2)}_{0.10}$, and $\mathbf{p(3)}_{0.10}$ under inhomogeneous illumination patterns.[26] Since Saphiannikova et al. have proposed photoinduced anisotropic stress as the origin of this bulk mass transport phenomenon,[46,47] it is of interest to correlate the photo-orientation of the complexes at the molecular level to their macroscopic photopatterning efficiency. Figure 4a shows that under the experimental conditions used (488 nm, interference pattern produced in a Lloyd's mirror interferometer using a circularly polarized beam of 50 mW/cm^2), the SRG formation efficiency, as determined by the first-order diffraction efficiency, increases in the order $\mathbf{p(2)}_{0.10}$ < $\mathbf{p(2)}_{0.25}$ < $\mathbf{p(1)}_{0.10}$ < $\mathbf{p(1)}_{0.25}$. A higher azobenzene content improves SRG formation for both complexes, but the halogen-bonded complex with a 0.10 azobenzene molar ratio outperforms the hydrogen-bonded complex with 0.25 azobenzene content. Comparing this to the molecular orientation values of Table 2, it is evident that the extent of polymer orientation does not directly correlate with the SRG forming capacity, although more pyridine orientation is induced in both systems when the amount of azo doping is increased from 0.10 to 0.25. Likewise, no direct correlation is found between the azobenzene molecular orientation and SRG diffraction efficiency, since higher azobenzene orientation is observed in the $\mathbf{p(x)}_{0.10}$ than in the $\mathbf{p(x)}_{0.25}$ complexes. However, although azobenzene photo-orientation decreases as a function of increasing degree of complexation, proportionally more pyridine groups will be affected in the $\mathbf{p(x)}_{0.25}$ as compared to the $\mathbf{p(x)}_{0.1}$ complexes. As shown in Figure 4c, the relative SRG formation efficiency of the different complexes correlates well with the weighted azobenzene orientation obtained by multiplying the measured photo-orientation of the azobenzenes by the number of chromophores per polymer chain to better represent the "anisotropic stress" generated in the material. In addition, the diffraction efficiency in the early stage of surface pattern formation (Figure 4b), which is known to result from the bulk photo-orientation grating,[48] is significantly higher for the $\mathbf{p(1)}_x$ complexes, in agreement with their higher photo-orientation

tendency. These results thus indicate a significant link between photo-orientation and all-optical surface-pattern formation, as previously suggested by a study of a series of azobenzenes ionically bonded to quaternized P4VP.[18]

Static IR spectroscopy with *in situ* illumination provides complementary information about the stability (changes in the association constant) of supramolecular bonds upon *trans*−*cis*−*trans* cycling, which is important for optimizing supramolecular materials for large photomechanical responses. Figure 5 shows IR spectra in the 993 cm^{-1} pyridine stretching vibration region for the $\mathbf{p}(\mathbf{x})_{0.25}$ complexes in the dark and under illumination of 160 mW/cm^2 of 450 nm unpolarized light. These illumination conditions ensure that the photoinduced anisotropy does not mask the photostability results and that the irradiance is higher than that used in photo-orientation and photopatterning experiments. In Figure 5a,b, it can be observed that, under irradiation, which creates a photostationary state that contains a large fraction of *cis* isomers (revealed by the *cis* band appearing at 880 cm^{-1}), the free pyridine absorbance at 993 cm^{-1} increases to a small but significant extent. Although the majority of the chromophores remain bonded under illumination and are thus able to photomechanically transmit the rotational energy to the pyridine units, the association constant between **1** and **p** slightly decreases under irradiation, which might increase the mobility of **1** in the matrix and be a key component for writing SRGs in supramolecular polymers with very low azobenzene content.[29] Figure 5c,d demonstrates that, in a similar manner, the equilibrium constant of hydrogen-bonded $\mathbf{p}(\mathbf{2})_{0.25}$ slightly decreases due to photoisomerization. The *cis* band at 880 cm^{-1} grows to a lesser extent than it does for $\mathbf{p}(\mathbf{1})_{0.25}$, in agreement with the lower *cis* content determined for the $\mathbf{p}(\mathbf{2})_{0.25}$ complex by UV−visible spectroscopy (Table 1). For $\mathbf{p}(\mathbf{3})_{0.25}$ (Figure 5e), a slight increase of the free pyridine band is observed upon irradiation and could be indirect evidence for a very weak hydrogen-bonding interaction between **3** and **p**. As expected, Figure 5f shows that the pyridine band at 993 cm^{-1} is unaffected by photoisomerization cycling for the nonbonding reference system, $\mathbf{p}(\mathbf{4})_{0.25}$.

In summary, the photo-orientation and photostability results indicate that the supramolecular bonds of $\mathbf{p}(\mathbf{1})_{0.25}$ and $\mathbf{p}(\mathbf{2})_{0.25}$ are stable enough to transfer partially the azobenzene motion to the polymer side chain but that illumination allows some azobenzene units to hop between adjacent repeat units or even between adjacent chains. This behavior was hypothesized to play an important role in the aforementioned study in which hydrogen-bonded complexes between **2** and **p** were capable of forming SRGs at the exceedingly low molar ratio of 1%.[29] In addition, our results are in good agreement with earlier work suggesting that there is a lower limit of hydrogen-bonding strength beyond which, at least in the solid state, hydrogen bonds become the dominant interactions over nonspecific van der Waals type interactions and other intermolecular interactions such as $\pi-\pi$ stacking, thus enabling the translation of photomechanical energy of azobenzenes into motion of passive molecules.[32] This work also suggests that halogen bonding is at least as effective as its more extensively studied hydrogen-bonding counterpart in photoresponsive materials, with the additional benefit of not plasticizing the polymer matrix.

CONCLUSIONS

This contribution provides an improved molecular-level understanding of why halogen-bonded photoactive supramolecular complexes often surpass the performance of corresponding hydrogen-bonded complexes in photomechanical applications, such as in all-optical surface patterning. Our results indicate that (i) choosing a supramolecular interaction of sufficient strength is important, since halogen and hydrogen bonding of −5.17 and −10.05 kcal/mol interaction strengths, respectively, are enough to provoke polymer orientation, whereas a weaker −3.5 kcal/mol hydrogen bond and a noninteracting azo dye do not; (ii) optimizing the degree of doping is essential, since there is a delicate balance between the azobenzene moieties orienting better at lower degrees of complexation and the polymer orientation and photopatterning efficiency improving at higher degrees of complexation; and (iii) the nature of the supramolecular bond is important, since complexation by halogen bonding, in contrast to hydrogen bonding, does not plasticize the polymer host due to the lesser mobility introduced by this noncovalent bond. These observations, especially in view of the almost identical photochemistry of chromophores **1** and **3**, strongly suggest that the physical properties of the matrix, such as its mobility measured by T_g, might well be a dominant, yet underaccounted for, parameter governing the optimal motion transfer of photoactive to passive molecules in solid-state applications.

ASSOCIATED CONTENT

Supporting Information

The Supporting Information is available free of charge on the ACS Publications website.

AUTHOR INFORMATION

Corresponding Authors

*(J.V.) E-mail: jaana.vapaavuori@umontreal.ca.

*(A.P.) E-mail: arri.priimagi@tut.fi.

*(C.P.) E-mail: c.pellerin@umontreal.ca.

Notes

The authors declare no competing financial interest.

ACKNOWLEDGMENTS

This work was supported by grants from the Natural Sciences and Engineering Research Council (NSERC) of Canada. J.V. is grateful to Emil Aaltonen Foundation, Finnish Cultural Foundation, and FRQNT for postdoctoral grants. I.T.S.H. is thankful for an Aalto Asci outgoing fellowship. We thank Calcul Québec and Compute Canada for providing access to the Briarée supercomputer. A.P. acknowledges the Academy of Finland and the Emil Aaltonen Foundation for financial support.

REFERENCES

(1) Bandara, H. M.; Burdette, S. C. *Chem. Soc. Rev.* **2012**, *41*, 1809−1825.

(2) Mahimwalla, Z.; Yager, K. G.; Mamiya, J.-i.; Shishido, A.; Priimagi, A.; Barrett, C. J. *Polym. Bull.* **2012**, *69*, 967−1006.

(3) Natansohn, A.; Rochon, P. *Chem. Rev.* **2002**, *102*, 4139−4176.

(4) Muraoka, T.; Kinbara, K.; Aida, T. *Nature* **2006**, *440*, 512−515.

(5) Norikane, Y.; Hirai, Y.; Yoshida, M. *Chem. Commun.* **2011**, *47*, 1770−1772.

(6) Yu, H.; Ikeda, T. *Adv. Mater.* **2011**, *23*, 2149−2180.

(7) Nagano, S.; Koizuka, Y.; Murase, T.; Sano, M.; Shinohara, Y.; Amemiya, Y.; Seki, T. *Angew. Chem., Int. Ed.* **2012**, *51*, 5884−5888.

(8) Sano, M.; Hara, M.; Nagano, S.; Shinohara, Y.; Amemiya, Y.; Seki, T. *Macromolecules* **2015**, *48*, 2217−2223.
(9) Rochon, P.; Batalla, E.; Natansohn, A. *Appl. Phys. Lett.* **1995**, *66*, 136−138.
(10) Kim, D. Y.; Tripathy, S. K.; Li, L.; Kumar, J. *Appl. Phys. Lett.* **1995**, *66*, 1166−1168.
(11) Yu, Y.; Nakano, M.; Ikeda, T. *Nature* **2003**, *425*, 145.
(12) Barrett, C. J.; Mamiya, J.-i.; Yager, K. G.; Ikeda, T. *Soft Matter* **2007**, *3*, 1249−1269.
(13) Priimagi, A.; Vapaavuori, J.; Rodriguez, F. J.; Faul, C. F. J.; Heino, M. T.; Ikkala, O.; Kauranen, M.; Kaivola, M. *Chem. Mater.* **2008**, *20*, 6358−6363.
(14) Kulikovska, O.; Goldenberg, L. M.; Stumpe, J. *Chem. Mater.* **2007**, *19*, 3343−3348.
(15) Marcos, M.; Romero, P.; Serrano, J. L. *Chem. Mater.* **2008**, *20*, 5209−5217.
(16) Xiao, S.; Lu, X.; Lu, Q.; Su, B. *Macromolecules* **2008**, *41*, 3884−3892.
(17) Zhang, Q.; Bazuin, C. G. *Macromolecules* **2009**, *42*, 4775−4786.
(18) Zhang, Q.; Wang, X.; Barrett, C. J.; Bazuin, C. G. *Chem. Mater.* **2009**, *21*, 3216−3227.
(19) Zhu, X.; Beginn, U.; Möller, M.; Gearba, R. I.; Anokhin, D. V.; Ivanov, D. A. *J. Am. Chem. Soc.* **2006**, *128*, 16928−16937.
(20) del Barrio, J.; Blasco, E.; Toprakcioglu, C.; Koutsioubas, A.; Scherman, O. A.; Oriol, L.; Sánchez-Somolinos, C. *Macromolecules* **2014**, *47*, 897−906.
(21) Gao, J.; He, Y.; Liu, F.; Zhang, X.; Wang, Z.; Wang, X. *Chem. Mater.* **2007**, *19*, 3877−3881.
(22) Priimagi, A.; Kaivola, M.; Virkki, M.; Rodríguez, F. J.; Kauranen, M. *J. Nonlinear Opt. Phys. Mater.* **2010**, *19*, 57−73.
(23) Sallenave, X.; Bazuin, C. G. *Macromolecules* **2007**, *40*, 5326−5336.
(24) Wu, S.; Duan, S.; Lei, Z.; Su, W.; Zhang, Z.; Wang, K.; Zhang, Q. *J. Mater. Chem.* **2010**, *20*, 5202−5209.
(25) Priimagi, A.; Cavallo, G.; Forni, A.; Gorynsztejn-Leben, M.; Kaivola, M.; Metrangolo, P.; Milani, R.; Shishido, A.; Pilati, T.; Resnati, G.; Terraneo, G. *Adv. Funct. Mater.* **2012**, *22*, 2572−2579.
(26) Saccone, M.; Dichiarante, V.; Forni, A.; Goulet-Hanssens, A.; Cavallo, G.; Vapaavuori, J.; Terraneo, G.; Barrett, C. J.; Resnati, G.; Metrangolo, P.; Priimagi, A. *J. Mater. Chem. C* **2015**, *3*, 759−768.
(27) Virkki, M.; Tuominen, O.; Forni, A.; Saccone, M.; Metrangolo, P.; Resnati, G.; Kauranen, M.; Priimagi, A. *J. Mater. Chem. C* **2015**, *3*, 3003−3006.
(28) Politzer, P.; Murray, J. S.; Clark, T. *Phys. Chem. Chem. Phys.* **2010**, *12*, 7748−7757.
(29) Koskela, J. E.; Vapaavuori, J.; Ras, R. H. A.; Priimagi, A. *ACS Macro Lett.* **2014**, *3*, 1196−1200.
(30) Zettsu, N.; Ogasawara, T.; Mizoshita, N.; Nagano, S.; Seki, T. *Adv. Mater.* **2008**, *20*, 516−521.
(31) Priimagi, A.; Cavallo, G.; Metrangolo, P.; Resnati, G. *Acc. Chem. Res.* **2013**, *46*, 2686−2695.
(32) Steiner, T. *Angew. Chem., Int. Ed.* **2002**, *41*, 48−76.
(33) Sourisseau, C. *Chem. Rev.* **2004**, *104*, 3851−3892.
(34) Buffeteau, T.; Pézolet, M. *Appl. Spectrosc.* **1996**, *50*, 948−955.
(35) Pézolet, M.; Pellerin, C.; Prud'homme, R. E.; Buffeteau, T. *Vib. Spectrosc.* **1998**, *18*, 103−110.
(36) Buffeteau, T.; Lagugné Labarthet, F.; Pézolet, M.; Sourisseau, C. *Macromolecules* **1998**, *31*, 7312−7320.
(37) Liang, Y.; Mauran, D.; Prud'homme, R. E.; Pellerin, C. *Appl. Spectrosc.* **2008**, *62*, 941−947.
(38) Roland, S.; Pellerin, C.; Bazuin, C. G.; Prud'homme, R. E. *Macromolecules* **2012**, *45*, 7964−7972.
(39) Natansohn, A.; Rochon, P.; Barrett, C.; Hay, A. *Chem. Mater.* **1995**, *7*, 1612−1615.
(40) Burland, D. M.; Miller, R. D.; Walsh, C. A. *Chem. Rev.* **1994**, *94*, 31−75.
(41) Priimagi, A.; Shevchenko, A.; Kaivola, M.; Rodriguez, F. J.; Kauranen, M.; Rochon, P. *Opt. Lett.* **2010**, *35*, 1813−1815.
(42) Labarthet, F. L.; Freiberg, S.; Pellerin, C.; Pézolet, M.; Natansohn, A.; Rochon, P. *Macromolecules* **2000**, *33*, 6815−6823.
(43) Toshchevikov, V.; Saphiannikova, M.; Heinrich, G. *J. Phys. Chem. B* **2009**, *113*, 5032−5045.
(44) Yadavalli, N. S.; Saphiannikova, M.; Santer, S. *Appl. Phys. Lett.* **2014**, *105*, 051601.
(45) Buffeteau, T.; Pézolet, M. *Macromolecules* **1998**, *31*, 2631−2635.
(46) Saphiannikova, M.; Neher, D. *J. Phys. Chem. B* **2005**, *109*, 19428−19436.
(47) Saphiannikova, M.; Toshchevikov, W.; Ilnytskyi, J. *Nonlinear Optics and Quantum Optics* **2010**, *41*, 27−57.
(48) Lagugné Labarthet, F.; Buffeteau, T.; Sourisseau, C. *J. Phys. Chem. B* **1999**, *103*, 6690−6699.